Chapter 5

Slowing and cooling of stored antiprotons in an ion trap

The task of slowing and cooling antiprotons 6 orders of magnitude in energy within an ion trap, from keV to meV, is accomplished by electron cooling which was first proposed in Ref. [4,61]. Electrons preloaded in a harmonic potential well cool via synchrotron radiation with a time constant 0.1 sec to thermal equilibrium at 4.2 K (corresponding kT = 0.36 meV). Antiprotons repeatedly pass through the electron cloud and collide with electrons until they fall into the harmonic potential well where the electrons reside. Within the well, antiprotons continue dissipating energies to electrons until thermal equilibrium is achieved between the antiproton and the electron clouds. Since the difference in the centrifugal barriers for antiprotons and electrons is approximately 2 K which is less than the thermal temperature 4.2 K, the centrifugal separation should not be a problem. This is the first demonstration of electron cooling in an ion trap. Since electron cooling is a nonresonant process, it can cool and slow antiprotons in a wide energy range without bandwidth limitation in contrast to resistor cooling and stochastic cooling. The cooling time of the order of seconds is much faster than any other technique [62]. Electron-antiproton collisions in the ion trap do not cause annihilations. Once antiprotons are confined in the harmonic potential well, resistor damping can be

also effective but slower than electron cooling. General discussions on the other antiproton cooling mechanisms can be found in Ref.[62].

5.1 Theory of electron cooling

In the degrader, antiprotons colliding with bound electrons cause dramatic energy loss as demonstrated in Chapter 2 where most of the 5.9 MeV antiproton kinetic energy is quickly transferred to the excitation and ionization energy of the initially bound electrons. In a metal target such as Al, the electron density is as high as $7.8\times10^{23}/cm^3$. A 5.9 MeV antiproton stops in Al in less than 20 ps at depth of about 0.25 mm. Collisions with a dense electron cloud confined in an ion trap would similarly slow antiprotons, but less rapidly.

A study of two species plasma (for example, an electron-proton gas) approaching thermodynamic equilibrium via collisions [63] was applied to an ion trap [62]. It is similar in some respects to the cooling of energetic particle beams using a collinear electron beam matched in velocity [64] and to the sympathetic cooling of one ion species by another in an ion trap [65]. If we assume electrons and protons both have Maxwellian velocity distributions, but with different kinetic temperatures T_e and T_p, the proton temperature will evolve with the following rate equation:

$$dT_p/dt = -(T_p - T_e)/t_c \tag{5.1}$$

where t_c, the time constant for equilibration of the temperatures, is given by

$$t_c = [3m_p mc^3/8(2\pi)^{1/2}n_e e^4 L][(kT_p/m_p c^2) + (kT_e/mc^2)]^{3/2}. \tag{5.2}$$

Values of L for an electron-proton gas are given in Ref.[63]. However, there are only a finite number of electrons in the trap and T_e is not a constant. An additional

rate equation for T_e is given [62]

$$dT_e/dt = [N_p(T_p - T_e)/N_e t_c] - (T_e - 4.2)/t_e \qquad (5.3)$$

where N_p and N_e are the total number of protons and electrons sharing the same volume, and t_e is the time constant for electrons energy loss due to synchrotron radiation and resistor damping. The rate equations were solved numerically for an electron density of $10^7/cm^3$, $t_e = 0.1$ sec, and an initial proton energy of 1 keV. The electron cooling times are of order 1 sec for different ratios of electrons and protons, $N_e/N_p = 10^2, 10^3, 10^4$ (Ref. [62]). (Note that we use E = kT/2 while E = kT was used in Ref. [62]).

The experimental conditions differed in several respects. The electron density is approximately $10^8/cm^3$. For the duty cycle D = 1, Fig. 5.1(a) shows the electron cooling processes for different ratios (10, 10^2, 10^3) of electrons to protons. The duty cycle that antiprotons interact with the electron cloud is about 3%, which causes the electron cooling time much longer. The t_c in Eqs. (5.1) and (5.3) should be replaced by t_c/D to include the duty cycle factor. Fig. 5.1(b) shows the electron cooling processes for D = 3%. The cooling time is approximately 11 sec for $D = 3\%$ and $N_e/N_p = 150$ (compared to 2 sec for D = 1). It is obvious that cooling times can not be linearly scaled. This is due to the large increase in the electron temperature, 10 times higher for D = 1 than for D = 0.03, which makes the cooling time longer. The time required to cool antiprotons from 1 keV to 100 K is plotted (Fig. 5.2) versus the electron density. There is an obvious inverse dependence on electron density for D = 0.03. This is less obvious for D = 1 due to the large increase in the electron temperature.

The calculation here and in Ref. [62] do not include the strong magnetic field used in the experiments. The calculation of electron cooling seems also valid for the presence of a strong magnetic field under the assumption that the axial and

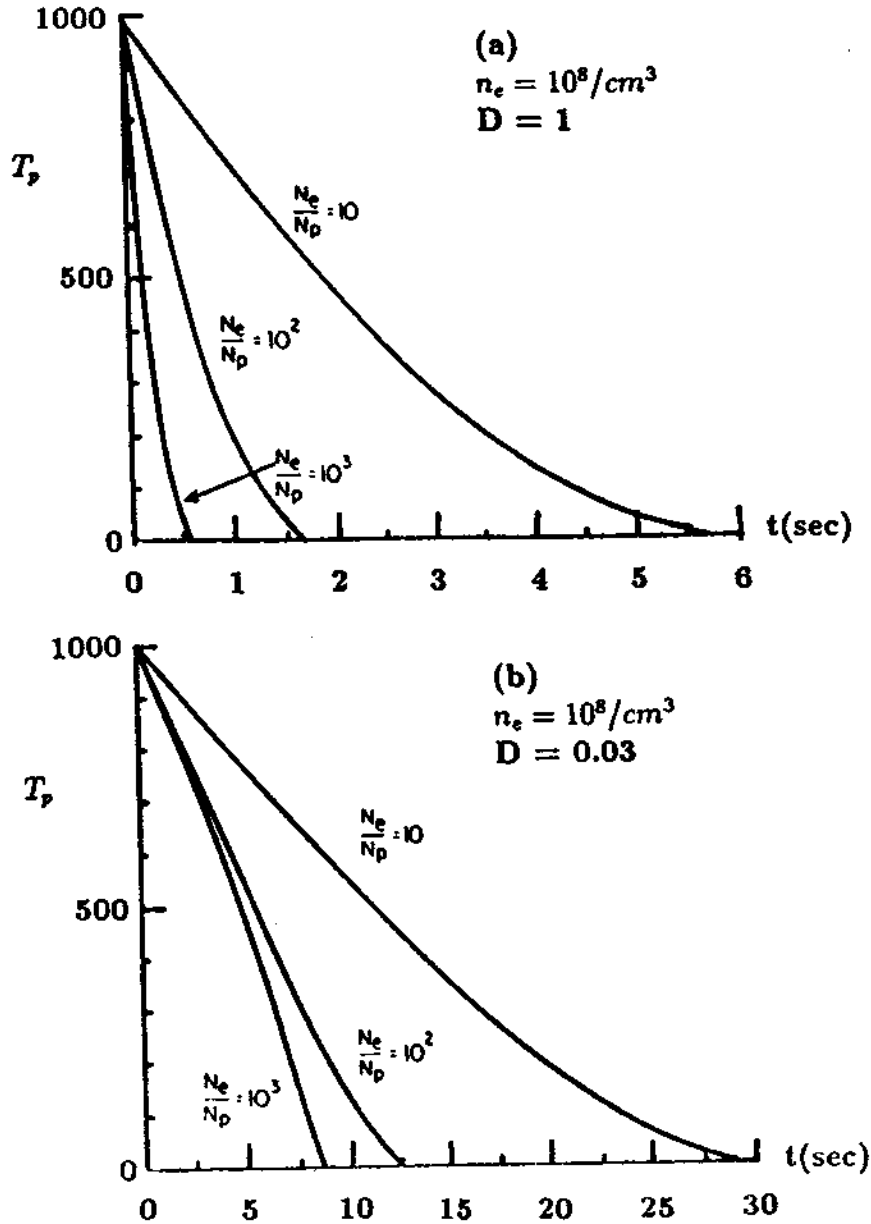

Figure 5.1: Calculation of the electron cooling processes for duty factor D = 1 (a) and 0.03 (b). The curves are calculated for different ratios of electrons to protons, as labeled.

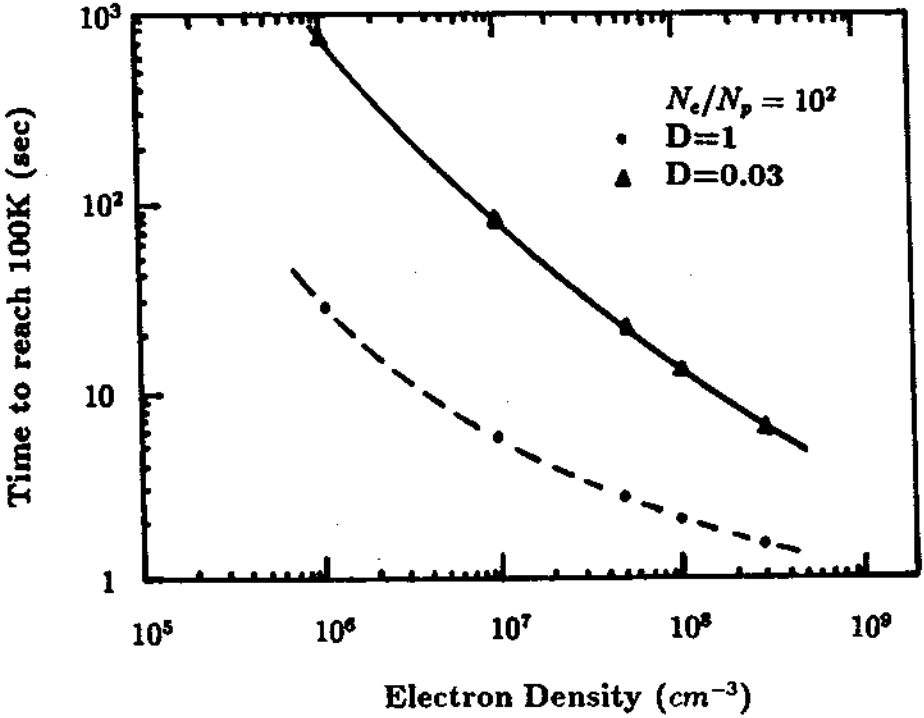

Figure 5.2: Electron cooling time versus electron density. The curves are included to aid the eye.

radial electron temperatures are equilibrated in the trap.

5.2 Experimental setup for antiproton slowing and cooling studies

The experimental setup for antiproton slowing and cooling studies is in Fig. 5.3. A field emission point (FEP) providing a primary electron beam in the trap is mounted above the upper cylinder. A series of rings form a long (13 cm) cylindrical trap which is shorter than the trap used in the antiproton trapping experiment (see Fig. 3.10) due to the relocation of the field emission point. Endcap electrodes can be at high negative potential for holding antiprotons within or at low positive potential so that antiprotons may escape and annihilate. The RCL circuit and FET amplifier on the upper compensation electrode detect a signal which is related to the number of electrons [66] when electrons are loaded in the harmonic potential well. To vary the well depth in the harmonic potential region or change its sign, we can expel the antiprotons and the electrons out. An antiproton annihilation detection system similar to the measurement of HV ramp antiproton energy spectrum (Chapter 3) is used.

5.2.1 Cylindrical open-endcap ion trap and ion motions

The cylindrical open-endcap ion trap is used for trapping electrons which are counted and monitored by RF techniques. It consists of a ring, two compensation and two open-ended endcap electrodes as shown in Fig. 5.4. The detailed calculation of its electrostatics is in Ref. [54]. The radius of the cylinder is $\rho_0 = 0.600$ cm. The length of the compensation electrode is $z_c = 0.489$ cm. The length from center of the ring to the edge of the endcap is $z_0 = 0.586$ cm. Gaps between the electrodes

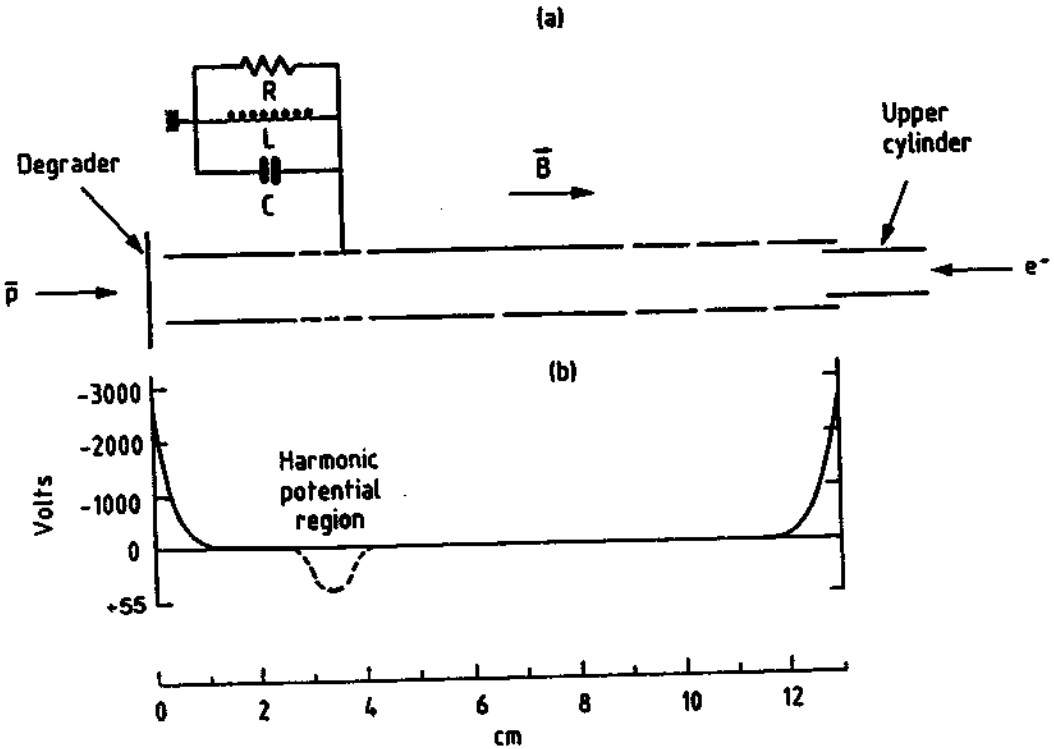

Figure 5.3: Experimental setup for antiproton slowing and cooling studies.

are 0.018 cm. The ring is at V_0 potential and the compensation potential V_c =0.88 V_0. The endcaps are grounded.

The electric potential V near the center of an ion trap can be expanded in Legendre polynomials,

$$V = (-V_0/2)\sum_{k=0}^{\infty} C_k (r/d)^k P_k(cos\theta) \tag{5.4}$$

where d is the characteristic length defined as $d^2 = (z_0^2 + \rho_0^2/2)/2$. All $C_{k=odd} = 0$ due to reflection symmetry across the z = 0 plane. Terms with $C_{k=even}$ depend on compensation potential V_c and trap geometry. C_0 represents the trap DC potential. The next lowest-order term, C_2 term, gives the needed harmonic quadrupole potential for axial confinement,

$$V_{C2} = -V_0 C_2 r^2 P_2(cos\theta)/(2d^2) = -V_0 C_2 (z^2 - \rho^2/2)/(2d^2) \tag{5.5}$$

The trap used for precision mass measurement has $C_2 = 0.5449$, and d = 0.512 cm. The potential energy for an antiproton of charge q = −e is

$$U(z,\rho) = qV = eV_0 C_2 (z^2 - \rho^2/2)/2d^2 = (1.04z^2 - 0.52\rho^2) \times 10^{-2} eV_0 \tag{5.6}$$

where z and ρ are in mm. For a single particle, its axial energy depends on axial position in a simple form $E = z^2 eV_0 \times 10^{-2}$. For example, the particle axial energy is 0.7 eV if its amplitude is 1 mm when the potential on the ring is 70 V. A particle will experience a harmonic well in axial direction while sitting on a potential hill in the radial direction. The corresponding axial frequency is given by

$$\omega_z^2 = C_2 eV_0/(md^2). \tag{5.7}$$

Existing higher order terms represent anharmonicity and they should be eliminated. As long as the particles are not far from the center of the trap, higher order terms diminish as k becomes larger. By adjusting the compensation potential, the anharmonic C_4 term can be tuned out to zero. A special choice of trap radius

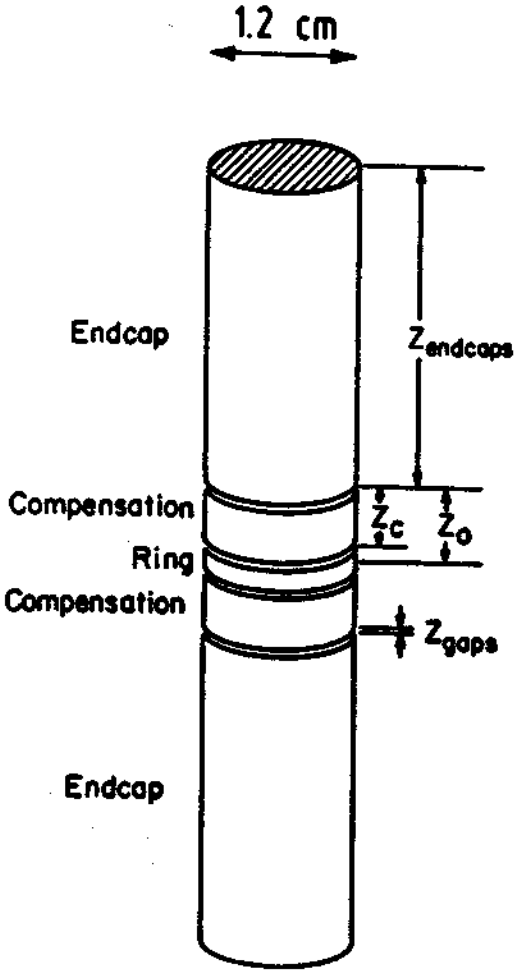

Figure 5.4: The cylindrical open-endcap ion trap (From Ref. [54]).

ρ_0/z_0 can minimize the axial frequency (or C_2) dependency on the compensation adjustment. In the ideal case, C_2 is independent of V_c and the trap with this feature is called an orthogonalized trap [67]. The higher order anharmonic C_6 term can also be eliminated in principle at $z_c/z_0 \approx 0.835$. In practice, a nonzero C_6 is expected due to the machining imperfections. Consequently, a harmonic potential can be realized in the center of the cylindrical compensated orthogonalized ion trap with open-ended endcap electrodes. The deviations from a harmonic potential due to trap machining and construction are unavoidable and their effects upon our precision measurement must be taken into account. The real trap used here is more complicated. The ring electrode is split into 4 identical segments and each compensation electrode is cut into 2 pieces along the z axis allowing various RF drives and detections to control and monitor the particles.

A particle of charge e and mass m is confined in a harmonic ion trap (i.e. a Penning trap) by applying a uniform magnetostatic field B parallel to the z axis for radial confinement and an electrostatic quadrapole potential for axial confinement. The electric potential that is a function of the cylindrical coordinates z and ρ is given by the Equation (5.5). The particle will harmonically oscillate along the z axis due to the axial electric field and travels in a circular cyclotron motion with frequency ω_c = eB/mc. However, this cyclotron motion is slightly modified by the repulsive radial component of the electric field. The modification results in an additional magnetron motion characterized by frequency ω_m (see Fig. 5.5). The particle motion is described by the relation:

$$z(t) = A_z cos(\omega_z t + \theta_z), \tag{5.8}$$

and

$$x(t) + iy(t) = |\mathbf{r}_m| e^{-i(\omega_m t + \theta_m)} + |\mathbf{r}_c| e^{-i(\omega_c' t + \theta_c)}, \tag{5.9}$$

where $\omega_z = \sqrt{C_2 e V_0 / m d^2}$, is the axial frequency, and

$$\omega_m = \omega_c/2 - \sqrt{(\omega_c^2/4) - (\omega_z^2/2)} \tag{5.10}$$

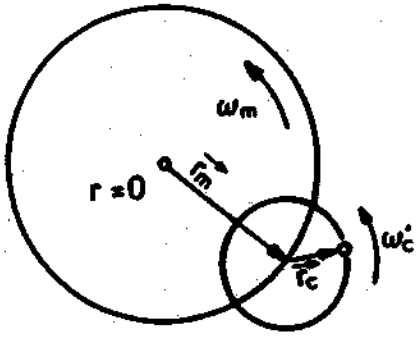

Figure 5.5: An antiproton radial motions in an ion trap (from Ref. [68]).

is the magnetron frequency, and

$$\omega_c' = \omega_c/2 + \sqrt{(\omega_c^2/4) - (\omega_z^2/2)} \tag{5.11}$$

is the modified cyclotron frequency. Then the cyclotron frequency is given as

$$\omega_c = \omega_c' + \omega_m, \tag{5.12}$$

where $\omega_m = \omega_z^2/2\omega_c'$. The center-of-mass motions for a cloud of ions are characterized by the same three frequencies and they are directly detected by our detection system discussed in the next section.

5.2.2 Preamplifier for the detection of ions and resistor damping

RF preamplifiers for particle resonant detection at a frequency range from 1 to 90 MHz, working at LHe temperature in 6 T field, are constructed. A GaAs field effect transistor (FET) MGF1100 (Mitsubichi Electronic) dual-gate n-channel Schottky gate type, is used. The dual gate configuration minimizes the Miller effect, an undesirable feedback between input and output of the FET that can degrade the high frequency performance of the device [69]. The electronic circuit is shown in Fig. 5.6. The first gate (G1) and the second gate (G2) of the FET are DC biased with RC filters. The source (S) is grounded and the drain (D) is biased at V_d. The signal from the RCL circuit goes to G1, then is amplified and goes through an impedance matching π-network to the next stage which has an input impedance of 50 Ω. The power gain is approximately 10^3 while the voltage gain is around one. The FET drain current is operated around 1 mA to keep the LHe boil-off low. Heat transferred to the liquid helium bath is 3 mW for $V_d = 3$ volts.

The amplifier is enclosed in a cylindrical copper cavity, 3.6 cm in diameter and 8.6 cm tall. A copper plate and a PC board with copper cladding on both sides

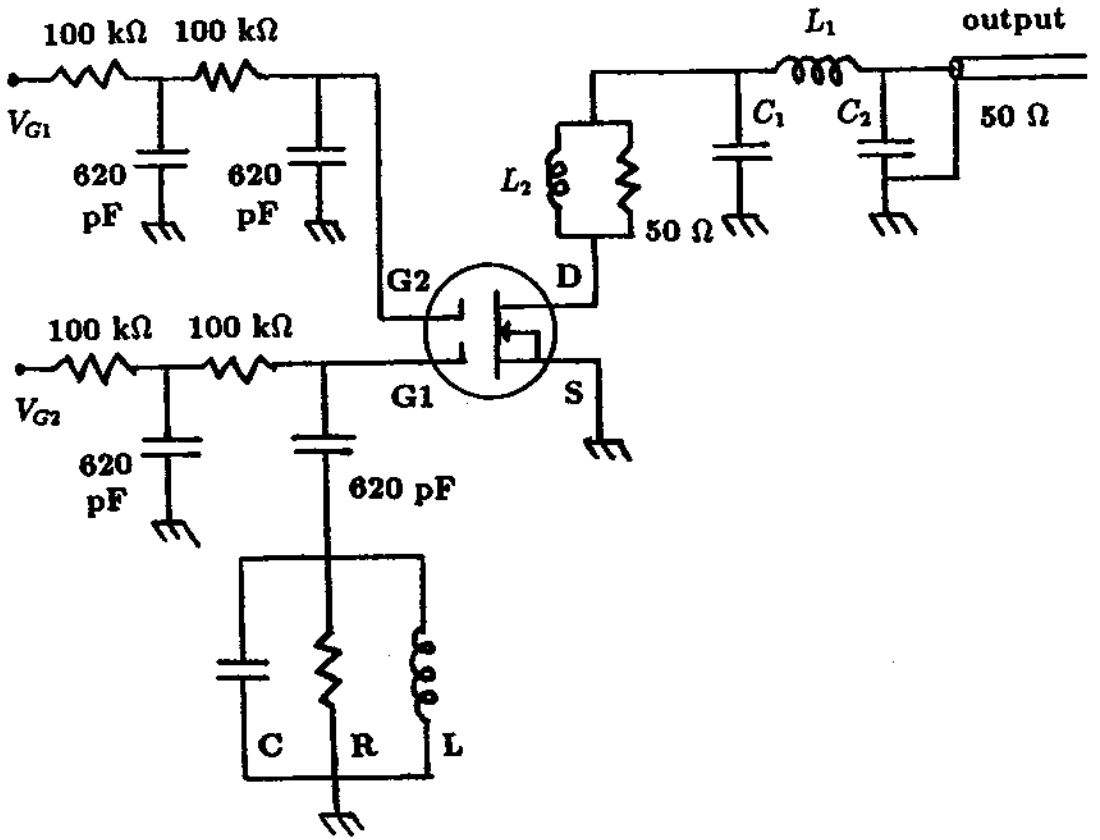

Figure 5.6: Dual-gate GaAs FET amplifier circuit.

separates it into two parts. The upper section (3.3 cm high) has the FET circuit in a vertical square PC board (3 cm× 3 cm). The cylindrical cavity below is 5 cm high with a diameter of 3.6 cm. It forms a resonator when it contains an inductor which can tune away the trap capacitance at the desired resonance frequency to achieve a pure resistive impedance. Helical resonators are discussed in Ref. [70,71]. A helical resonator for frequency at 30 to 90 MHz consists of 6 to 3 turns of silver plated copper wire with diameter of about 2 mm. For low frequencies, 1 to 3 MHz, the inductor wires are enamelled wire with more than 100 turns. The capacitance C in Fig. 5.6 includes the effective distributed capacitance, the capacitance of the feedthrough, and the contribution from the trap electrodes. The resistive loss in the LC circuit is inversely proportional to an effective resistance R in parallel with the LC at the resonant frequency. It is desirable to keep the distributed capacitance to a minimum and to keep the inductance high for best performance.

The Johnson noise RMS voltage for a resistor R at temperature T is, $V_{RMS} = \sqrt{4kRTB}$, where B is the bandwidth, and k is the Boltzmann constant. We use Q, the quality factor of the parallel-resonant circuit, as a measure of resistive loss. Q value is

$$Q = f/\Delta f, \tag{5.13}$$

where f is the center frequency of the noise resonance, and Δf is the FWHM of noise signal in power, or half-power bandwidth, which corresponds to a width at 70% of the amplitude in RMS voltage scale. The peak of RMS voltage across the LCR circuit corresponds to the Johnson noise. A noise resonance at 68 MHz, for a FET preamplifier at LHe temperature, is shown in Fig. 5.7(a). It has a Q value of 500. The relations of Q with R, C, and L can be expressed as:

$$Q = R/\omega L = RC\omega \tag{5.14}$$

The higher the Q of the circuit, the higher the parallel impedance R at the resonant frequency.

As the particle oscillates in the trap axially and radially the image current I_{ind} flows and dissipate energy through a resistor R between an electrode and ground. The potential signal $V_s = I_{ind}R$ can be detected by a preamplifier. The induced current by axial motion, observable in the compensation electrode, is $I_z = k_z e\omega_z z/2z_0$, where k_z is a constant of order one related to the trap geometry,z is the amplitude of the particle axial oscillation. For the trap we are using, k_z is calculated to be 0.8994 [54]. It is smaller (0.3346) when the detection is the from the endcap electrode.

Since the circular motion can be viewed as two superimposed harmonic oscillators, an induced current on one segment of the ring electrode is in similar form $I_c = k_c e\omega_c \rho_c/2\rho_0$. For a fixed geometry and motion frequencies, it is understandable that a large amplitude of oscillation would bring a large signal. In reality, because capacitance exists between each pair of electrodes, a pure resistance can only be achieved when an inductor tunes away the capacitance at a certain resonant frequency. The kinetic energy of the particle coupled to the resistor decreases until the particle is in thermal equilibrium. The power is dissipated in the resistor generating heat. As an example for axial motion, energy loss in the effective resistance R damps the particle motion with a damping time constant given by [72]

$$\tau = (m/R)(2z_0/ek_z)^2 \tag{5.15}$$

where e and m are the charge and mass of the particle. Because the time constant is proportional to the mass, resistor damping is 3 orders of magnitude more effective for an electron than for a antiproton when other conditions are equal. For a typical value of R = $10^5\Omega$, the time constant for an electron is approximately 0.1 sec while it is 100 sec for an antiproton. The cooling of a cloud of particles can not be faster than a single one due to internal degrees of freedom of the axial and cyclotron motion [62].

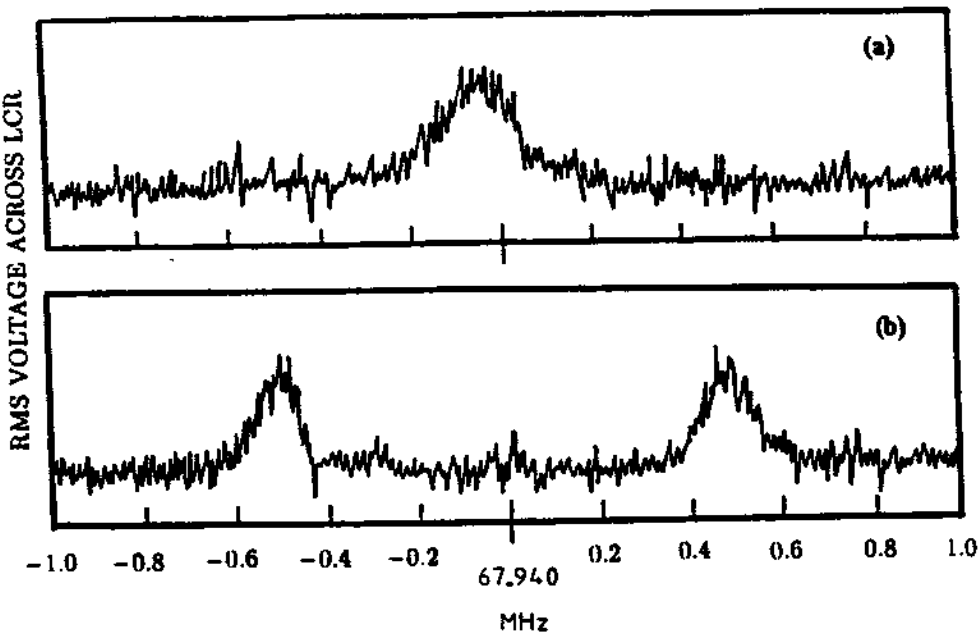

Figure 5.7: (a) Typical noise resonance for the LCR circuit at LHe temperature. (b) Modified signal when large electron cloud is present. The spacing of the two peaks of 1 MHz indicates that 6×10^6 electrons are in the trap.

The effective radio-frequency circuit used to damp and detect the ion motion can be represented as shown [73] in Fig. 5.8. An oscillating particle with charge e induces a current I through the resistor R when an inductor is used to tune out the trap capacitance. V_n is the Johnson noise from the resistor which is proportional to the square root of R, $\sqrt{R}$. V_s is the input voltage signal detected by a preamplifier. The particle motion can be driven by the oscillatory potential V_D continuously or just for a short period then switched off. The Johnson noise is "shorted out" on resonance [66].

The number of electrons can be counted from axial detection [66]. The linewidth of a single particle is given by $\Delta f_1 = 1/(2\pi\tau)$. The noise from the center of the spectrum is shorted for particles oscillating at the frequency $f = 1/2\pi\sqrt{LC}$ in the trap. Two resonant peaks are formed as in Fig. 5.7(b) for large numbers of electrons when the width between two peaks $\Delta f_N >> \Delta f$, the width of the noise resonance. The position of the peaks corresponds to the parallel resonances formed when the reactive impedance of the electrons is equal and opposite to the reactive impedance of the external tank circuit [66]. In this case the numbers of electrons is given by

$$N = (\Delta f_N)^2/(\Delta f_1)(\Delta f). \tag{5.16}$$

In Fig. 5.7(b), the numbers of electrons N is approximately 6×10^6 for $\Delta f_N \approx 1$ MHz, $\Delta f_1 \approx 1.2$ Hz, and $\Delta f \approx 135$ kHz. The electron density will be discussed in section 5.3.

5.2.3 Selectively ejecting electrons and antiprotons

The trapping potential is switched from V_0 to a low voltage between 0 to 4 V in approximately 5 ms and stays there for approximately 0.6 sec, then goes

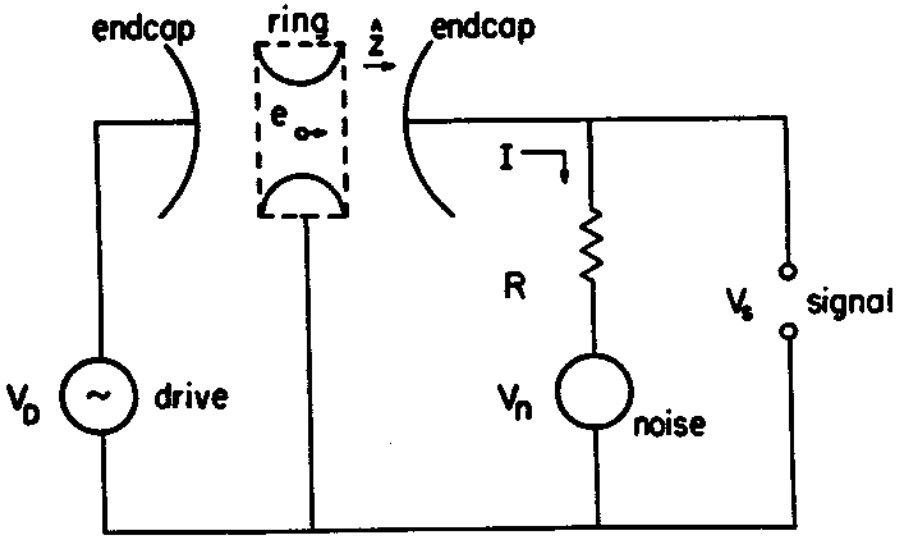

Figure 5.8: Detection and resistor damping of ion motion (from Ref. [73]).

back to the initial potential. This is a called potential dip. The ratio of electron number to antiproton number can be changed by the dip process combined with RF drive on the electron frequencies ν_z and $\nu_z + \nu_m$. The low voltage linear ramp can eject the trapped particles and the antiproton number can be measured by this destructive method. The low voltage dip/ramp circuit is shown in Fig. 5.9(a). When the TTL signal controlled relay switch S_1 is at position A and C, the normal ring potential V_0 and the compensation potential V_c are applied to the trap. The TTL signal controlled relay switch S_2 can be chosen to connect the dip potential V_{dip} or the ramp potential V_{ramp}. When S_1 is switched to position B and D, the V_{dip} is applied to the trap electrodes. If S_2 is also switched from position F to E when S_1 is switching, the low voltage ramp is applied to the trap electrodes. After 0.6 sec, the trap potentials are back to V_0 and V_c when S_1 is reset to position A and C. The resistors are used to keep $V_c = 0.88V_0$ for the harmonic potential well. A typical potential dip waveform on the ring electrode is shown in Fig. 5.9(b). A typical potential ramp waveform on the ring electrode is shown in Fig. 5.9(c). The ring potential V_0 first drops to 10 V, then ramps down to below -5 V in 560 ms with a linear ramp rate of 30.3 mV/ms. The potential well depth (at the center of the trap) has a ramp rate of 23.5 meV/ms.

Just like the detection system for the HV ramp in the long trap described in Chapter 3, another identical multiscaler is triggered and starts counting the antiproton annihilations when the harmonic potential well changes. Particles with energies exceeding the well leak out and their annihilations are detected as an energy spectrum. As an example, Fig. 5.10 shows the energy spectrum of antiprotons released from the harmonic trap with a linear ramp. It has 190 counts of antiproton annihilations (representing 400 antiprotons) and a width of 5 meV. Actually the width is approximately equal to the time resolution of 1 channel per 0.2 ms in the Joerger multiscaler.

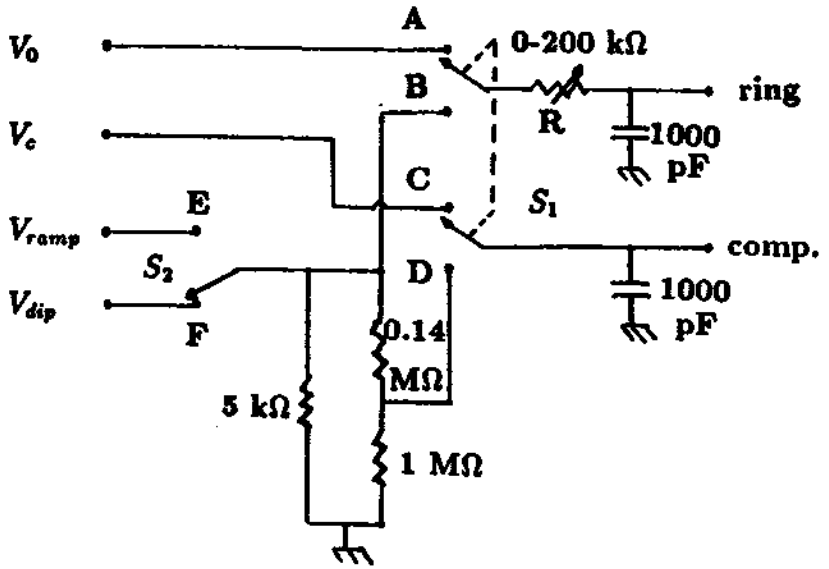

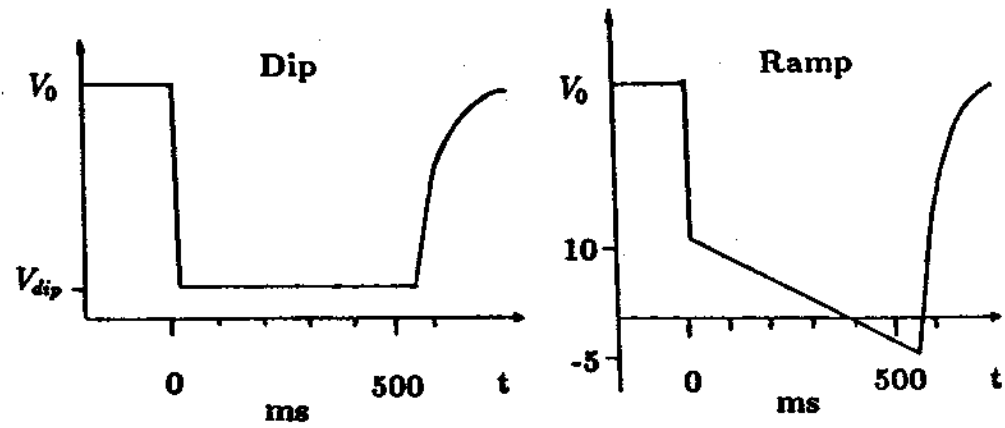

Figure 5.9: Low voltage dip/ramp circuit and its waveforms.

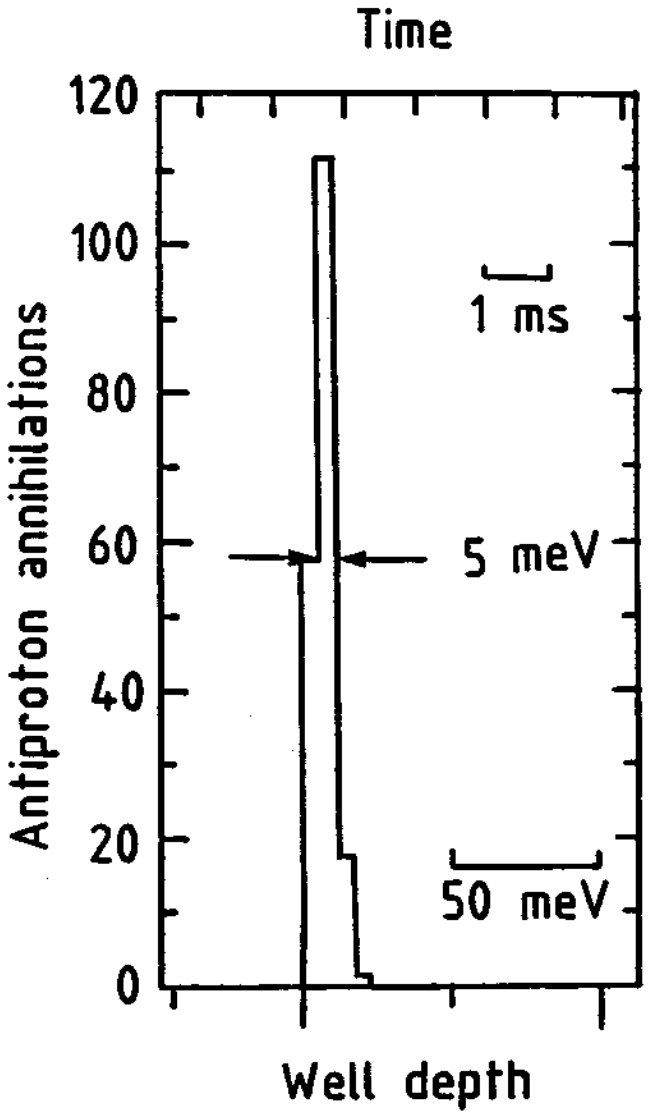

Figure 5.10: Antiproton energy spectrum after particles are ramped out from harmonic well.

5.3 Electron cooling studies

A large and dense electron cloud is needed for rapid cooling and slowing of the antiprotons. A beam of energetic electrons from the field-emission point strikes the degrader and causes the release and later the ionization of neutral atoms. The stripped electrons as well as the secondary electrons emitted directly from the degrader surface are confined in the harmonic potential well. The electron density can be estimated in a simple model where the electron cloud forms a sphere and the Coulomb repulsion balances the axial electrostatic field. In the harmonic trap used here, this gives an electron density $n_e \approx 3.5 \times 10^6 V_0/cm^3$. It is $10^8/cm^3$ for the applied potential $V_0 = 30$ V. The diameter for a cloud of 6×10^6 electrons given by this simple model is approximately 0.5 cm.

The electron cloud is an unneutralized electron plasma. Its Debye length is 1.4×10^{-3} cm which is much smaller than the cloud size. The electron plasma frequency is 92 MHz for $V_0 = 30$ V (it is 140 MHz at 70 V). The parameter $\Gamma = e^2/akT = 0.2$ (a = 2×10^{-3} cm is the particle spacing) is much smaller than 2 which is required to form a liquid plasma [74].

5.3.1 Antiproton-electron collisions and energy loss

Antiprotons moving through the cold electron cloud lose energy by antiproton-electron collisions. Eventually, the antiprotons fall into the harmonic potential well and form a new bound state after their initial kinetic energies are transferred to the electrons. We denote N_h as the number of hot antiprotons remaining in the long trap. The number of cooled antiprotons N_c which fall into the harmonic well by electron cooling is measured by decreasing the potential of the harmonic well crossing 0 V as shown in Fig. 5.9. The total number of trapped antiprotons is $N = N_h + N_c$ (on the order of 10^4). Fig. 5.11 shows the fraction of hot antiprotons

(N_h/N) and cold antiprotons (N_c/N) versus the cooling time. The time allowing hot antiprotons colliding with cold electrons is increasing, the hot fraction is getting smaller while the cold fraction larger. There are 4×10^6 electrons (the width of the clouds is 0.8 MHz) in the center of the harmonic trap covering a large fraction of the diameter of the trap so that nearly 100% of the antiprotons are cooled into the harmonic well for cooling times exceeding 100 seconds. Generally, the scattering of the points are small. The observed fluctuations are larger if we normalize to the initial PPAC signals which are proportional to the number of antiprotons delivered by LEAR. This is due to the missteering of the beam since the PPAC signals are not exactly proportional to the total numbers of trapped antiprotons under such condition.

The fraction of antiprotons cooling into the harmonic potential well for various numbers of electrons in the trap versus cooling time is shown in Fig. 5.12. The curves are included to aid the eye. Up to 95% of the antiprotons trapped in the long trap fall into the harmonic well after 100 sec. The time constant for the cooling process is about 10 sec when 4×10^6 electrons are preloaded in the ion trap, which is in good agreement with our estimate in Sec. 5.1. Thus a rapid cooling and slowing of antiprotons are achieved. As the number of electrons is reduced, electron cooling is less effective because the interaction region with antiprotons are smaller. Many factors limit a more quantitative comparison with Spitzer's theory. Beside the magnetic field mentioned in Sec. 5.1, there may be a difference between electron-proton collisions and electron-antiproton collisions since we have observed such difference in the proton and antiproton range measurements (see Section 2.5). Energies in radial motion are not measured here. Electrons heated by antiprotons with axial energy above 3 keV (antiprotons which are not trapped) contribute a larger electron temperature and a longer cooling time. The particle distribution for both electrons and antiprotons is not a Maxwell-Boltzmann distribution.

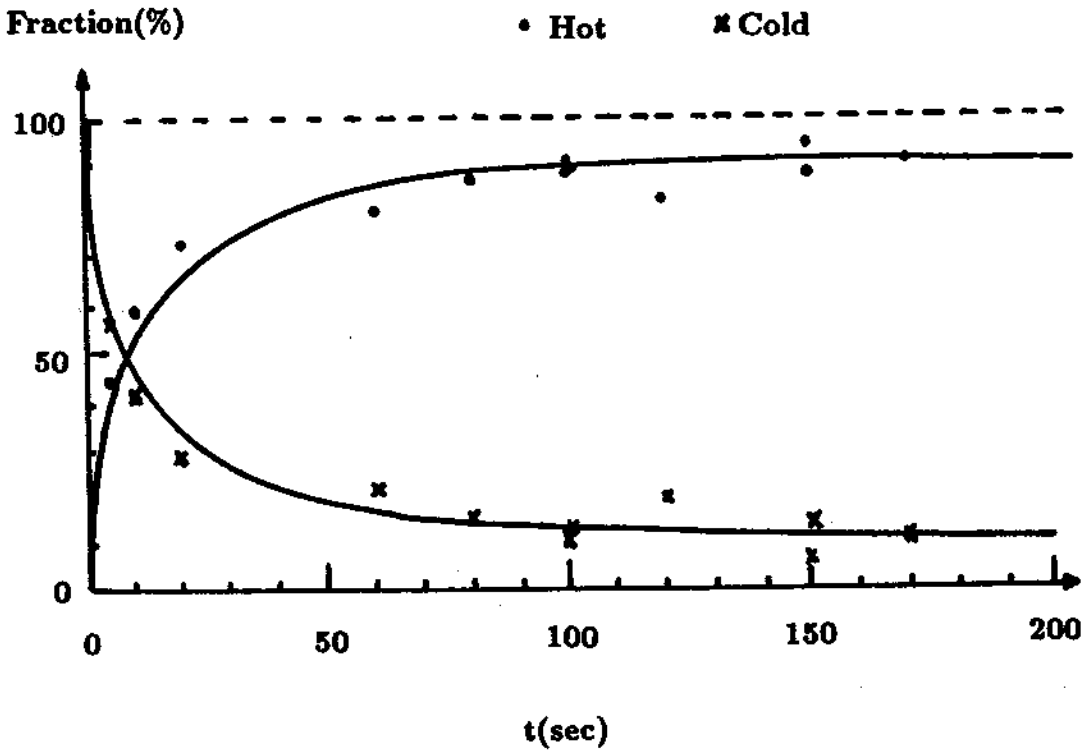

Figure 5.11: Fraction of hot antiprotons and cold antiprotons versus the cooling time. The curves are included to aid the eye.

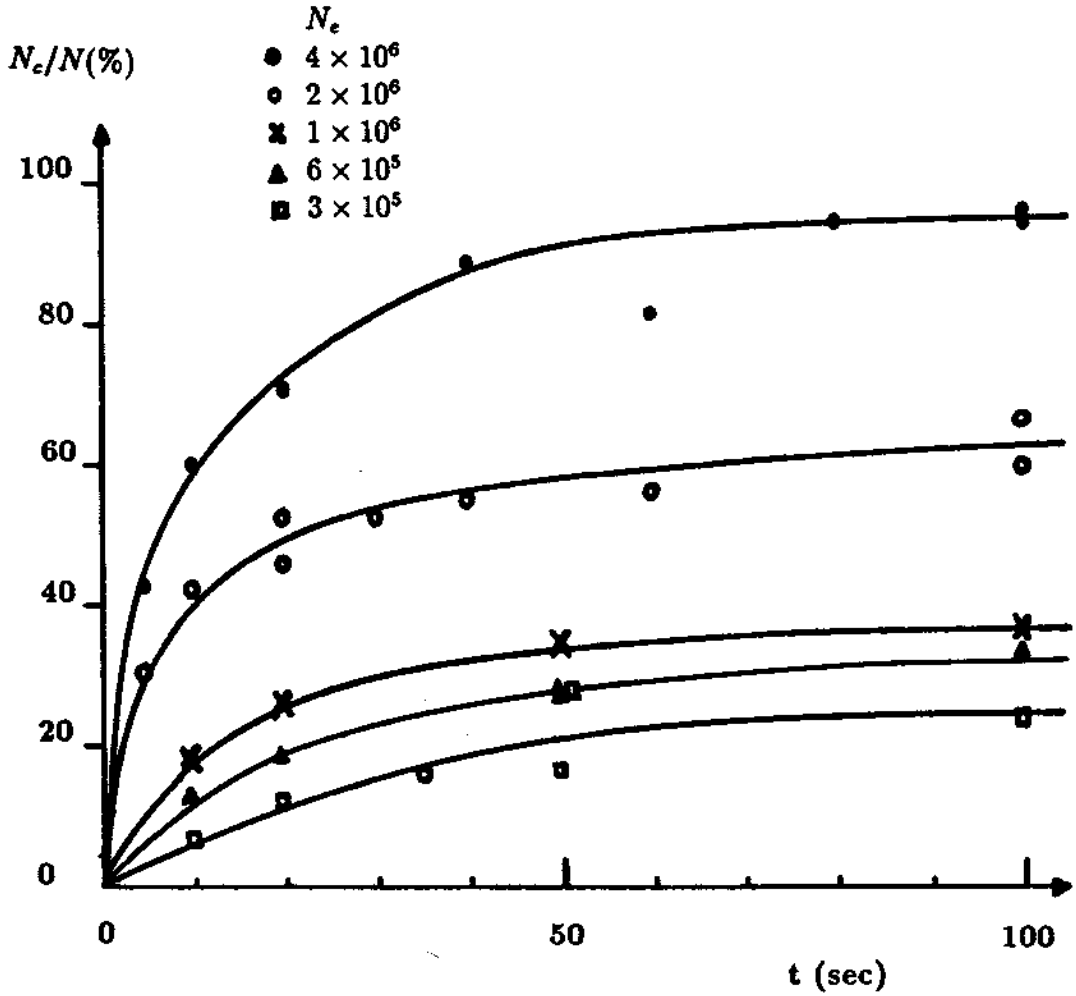

Figure 5.12: Fraction of antiprotons falling into the harmonic potential well for different numbers of electrons in the trap versus cooling time. The curves are included to aid the eye.

5.3.2 Low energy antiproton ramp spectrum

The width of the low energy antiproton ramp spectrum is due to the space charge of the antiproton cloud. In the trap we use, a crude estimate approximately given by

$$E = 0.069 N^{2/3}\ meV. \tag{5.17}$$

In Fig. 5.13, we have three examples of the number of antiprotons detected escaping the harmonic well as a function of the well depth. The well depth is reduced linearly in time at the rates indicated in the insets. Electrons used for cooling are still in the trap (a) and most have been removed for (b). In (c), the number of antiprotons has been reduced as well. It is not surprising to see low energy tails in all the energy spectra because some particles can be very cold. The high energy tail only becomes obvious when large number (millions) of particles are present as seen in (a). In the example (a) where 14,000 antiprotons annihilation counts (or 3×10^4 antiprotons) are detected, the depth of the harmonic well is decreased from 23 eV to below 0 eV at a rate of 23.5 meV/ms, with each channel 1 ms. The zero crossing is hard to locate precisely since stray potentials within the electrodes are expected to shift the well depth by as much as 30 meV. The observed width is 84 meV (the energy width of 66 meV is estimated using Eq. (5.17)). In the example (b), the width is 37 meV for 1.6×10^4 antiprotons (the width of 44 meV is estimated), with each channel 0.2 ms, after most of the electrons are resonantly ejected from the trap. If in addition we reduce the number of antiprotons in the trap to approximately 850 (6 meV is estimated) or 400 (4 meV is expected), the observed width decreases to only 9 meV (Fig. 5.13(c)) or 5 meV (Fig. 5.10). The observed energy width agrees with the Eq. (5.17) very well. Because there is a broad shoulder at left side of the peak in (a), the width can not be compared directly with the spectra without this shoulder. The electron spectrum is not measured.

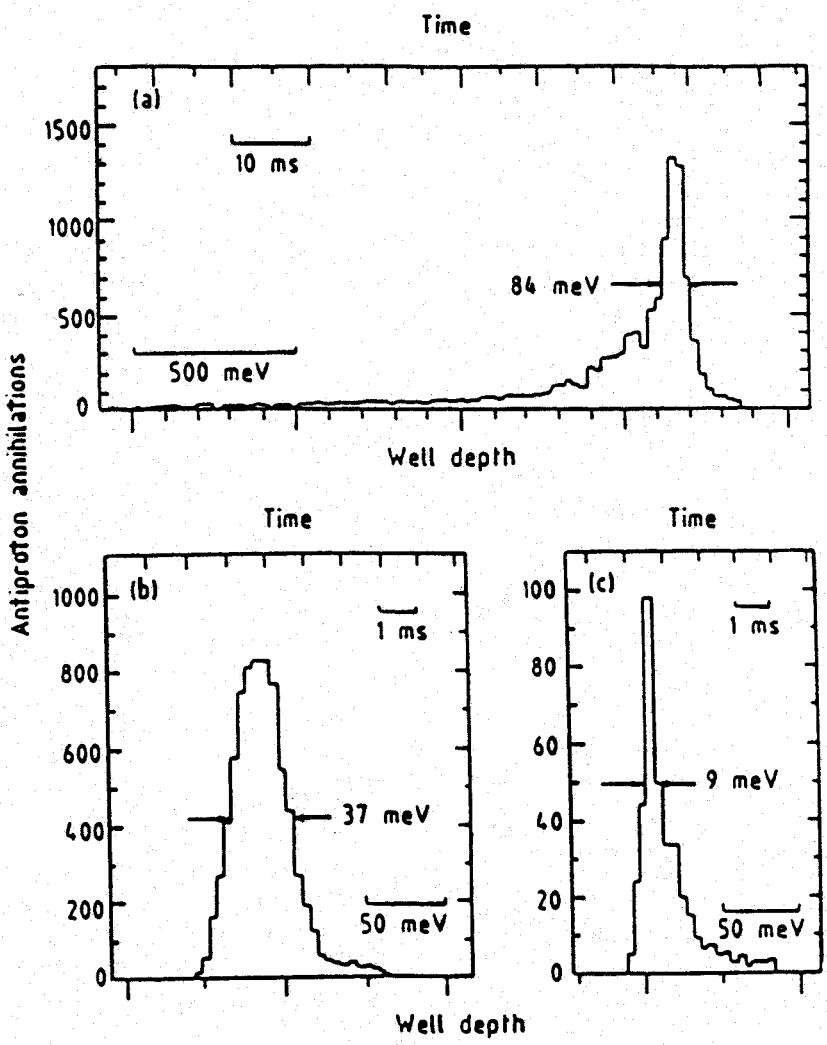

Figure 5.13: Low voltage dump spectrums.

The energy spectrum can change depending on the RF drive strength and frequency (how close it is to resonance) just before antiprotons are dumped. A strong RF drive can make the high energy tail in Fig. 5.13(a) much larger and the particle distribution is also shifted to higher energy. The energy spectrum of a heated antiproton cloud (8500 antiprotons) is shown in Fig. 5.14. Before the antiproton dump, axial and cyclotron signals (the nondestructive resonant method will be discussed in Chapter 7) stay hot for more than 30 minutes after the cyclotron drive was turned off, which is an indication that there are not many electrons in the trap. Comparing Fig. 5.14 and Fig. 5.13(b) shows the effect of the heated antiproton cloud. The dump energy spectrum in Fig. 5.14 shows a large number of hot particles are between 0.1 and 1 eV, that are absent in Fig. 5.13(b). There was no strong drive during the low voltage dump. The particle energy distribution with large high energy tail is due to the heated antiproton cloud in the trap with a large spacial distribution.

5.3.3 Cryogenic antiprotons at 4.2 K

We have discussed that antiprotons could dissipate energy by resistor cooling. As shown in Fig. 5.15, the detected power signal for cyclotron motion which is proportional to the cyclotron motion center-of-mass energy versus time by resistor damping is given. The time constant is about 20 minutes which is much longer than the calculated cyclotron damping time (τ_1) for single particle of 3 minutes, because of the additional time needed for energy transfer from internal motions to the center-of-mass motion for a cloud of antiprotons. If the internal motions are absent, the damping time constant for the center of mass motion for N particles is τ_1/N. When there are some electrons in the trap with antiprotons, the damping time can be much faster ranging from seconds to minutes. The dash line in the figure represents an electron damping curve with a time constant of 1 minute. The

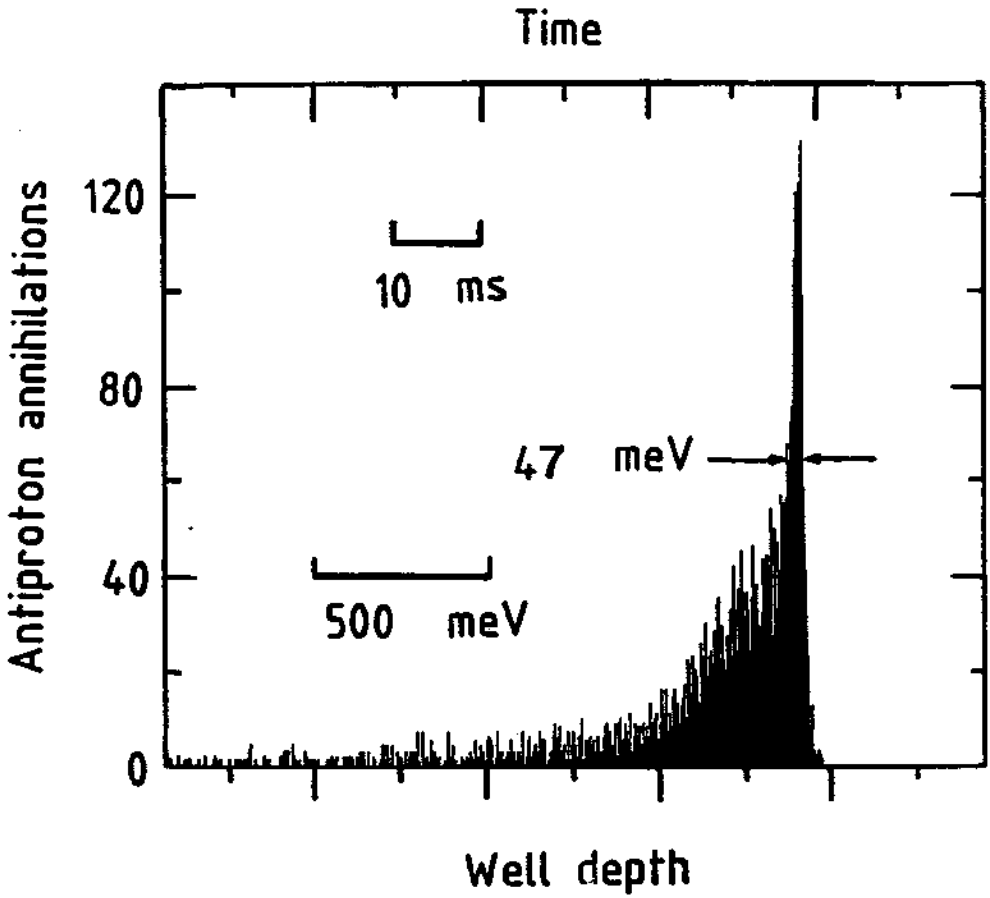

Figure 5.14: The energy spectrum of a heated antiproton cloud.

trap and its vacuum enclosure are cooled down to LHe temperature. The thermal equilibrium temperature is presumably achieved when there is no external heating source. Both damping mechanisms can make antiproton axial motion reach thermal equilibrium. For trapped antiprotons in thermal equilibrium with their surroundings, their thermal energy 3kT/2 is 0.54 meV for T = 4.2 K. Trapping and cooling low energy antiprotons in an ion trap have been demonstrated here. Important applications will be discussed in Chapter 6 and 7.

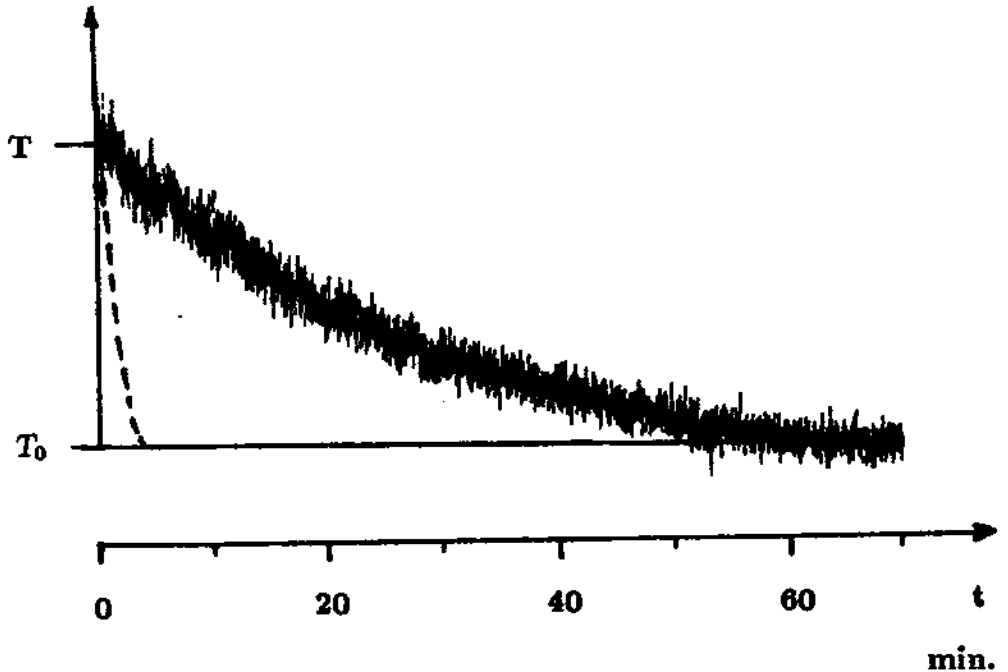

Figure 5.15: Resistor damping the antiproton cyclotron motion. Electron damping is many times faster (dash line).